Journal of Molecular Structure 1012 (2012) 1–11

Contents lists available at SciVerse ScienceDirect

Journal of Molecular Structure

journal homepage: www.elsevier.com/locate/molstruc

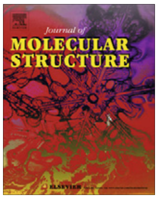

Synthesis, molecular structures and phase transition studies on benzothiazole-cored Schiff bases with their Cu(II) and Pd(II) complexes: Crystal structure of (E)-6-methoxy-2-(4-octyloxy-2-hydroxybenzylideneamino)benzothiazole

Guan-Yeow Yeap [a,*], Boon-Teck Heng [a], Nur Faradiana [a], Raihana Zulkifly [a], Masato M. Ito [b], Makoto Tanabe [c], Daisuke Takeuchi [c]

[a] *Liquid Crystal Research Laboratory, School of Chemical Sciences, Universiti Sains Malaysia, 11800 Minden, Penang, Malaysia*
[b] *Department of Environmental Engineering for Symbiosis, Faculty of Engineering, Soka University, Hachioji, Tokyo 192-8577, Japan*
[c] *Chemical Resources Laboratory (Mailbox R1-03), Tokyo Institute of Technology, 4259 Nagatsuta, Midori-ku, Yokohama 226-8503, Japan*

ARTICLE INFO

Article history:
Received 22 July 2011
Received in revised form 28 December 2011
Accepted 28 December 2011
Available online 4 January 2012

Keywords:
Cu(II) complexes
Pd(II) complexes
FTIR
NMR
Single crystal X-ray diffraction
Mesomorphic behaviour

ABSTRACT

Two new homologous series of Cu(II) and Pd(II) complexes with benzothiazole-cored Schiff bases have been synthesised with the aim to study the mesomorphic and thermal properties of ligands upon formation of metal complexes. The molecular structure of title compounds were elucidated with the employment of FT-IR, 1D and 2D FT-NMR spectroscopic techniques. Mesomorphic and thermal behaviour of title compounds have been investigated by differential scanning calorimetry and polarising optical microscope. All the ligands are nematogenic but the corresponding Cu(II) and Pd(II) complexes crystallised in ordinary solid. The conformation of 6-methoxy-2-(4-octyloxy-2-hydroxy-benzylideneamino)benzothiazole was determined by single crystal X-ray diffraction analysis of which the title compound favours more stable (**E**)-6-methoxy-2-(4-octyloxy-2-hydroxybenzylideneamino)benzothiazole. Crystal structure of the title compound also revealed that the bond length of C=N (1.303 Å) in the benzothiazole rings very close to that in the exocyclic C=N linkage (1.298 Å).

1. Introduction

A considerable number of metallomesogens and their properties have extensively been studied in recent years [1]. The presence of metal ions, particularly the transition metals, was found to be more superior than the free ligands owing to the advantages of combining the properties of these ligands with transition metals. In general, the incorporation of metal ions will help to reinforce the anisotropic behaviour of these ligands which resulted in the conversion of the non-mesogenic ligands to complexes which possesses liquid crystalline properties [2]. Besides, the resulting metal complexes are claimed to be more polarisable and the complex molecules may become suitably oriented for the fortification properties [3].

In 2005, Patel and Bhattacharya found that even though the free tetradentate Schiff base exhibit liquid crystalline properties, the corresponding binuclear Cu(II) and Ni(II) complexes are non-mesogenic. The observation shows that the incorporation of metal ion reduced or diminished the anisotropic properties of the ligand. This effect may due to the unfavourable orientation and the polarisability of the resulting complexes [4].

The introduction of heterocyclic unit within the central core of calamitic molecules has commonly been regarded as an interesting strategy to design liquid crystal compounds [5]. The heterocyclic unit usually involved five or six member ring with heteroatoms like S, O and N which are considered more polarisable than carbon [6]. Thus, the heteroatoms can change liquid crystalline phase and the physical properties of the observed phase [7]. Recently, heterocyclic liquid crystal compounds have been studied for application such as thiophenyl-based liquid crystalline compounds for non linear optic materials and benzothiazolyl-based liquid crystalline compounds for photoconductive materials [8]. In addition, benzothiazole is a kind of heterocyclic fused ring system which has been widely studied as they exhibit interesting photophysical and fluorescent properties [6]. It has also been proven as an effective core in mesogens [7]. In this paper, we focus on the studies of 2D NMR for benzothiazole-cored Schiff bases ligands and the crystal structure for 6-methoxy-2-(4-octyloxy-2-hydroxybenzylideneamino)benzothiazole. We also describe the influence of Cu(II) and Ni(II) ion upon the mesomorphic and thermal properties of ligands.

---

* Corresponding author. Fax: +60 4 6574854.
E-mail addresses: gyyeap@usm.my, gyyeap_liqcryst_usm@yahoo.com (G.-Y. Yeap).

0022-2860/$ - see front matter © 2012 Elsevier B.V. All rights reserved.
doi:10.1016/j.molstruc.2011.12.048

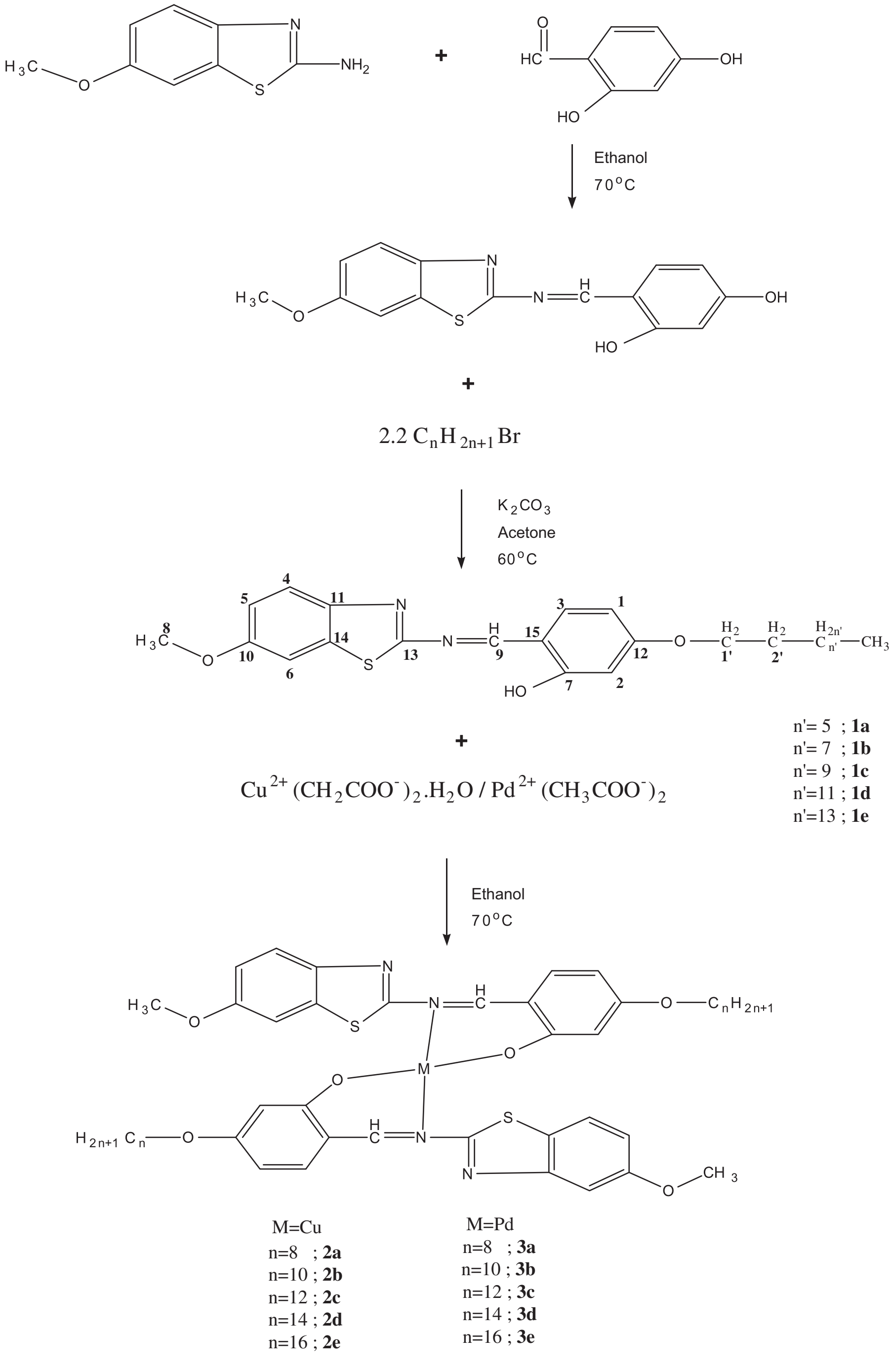

Scheme 1. Synthetic route towards formation of ligands **1a–1e** with their complexes **2a–2e** and **3a–3e**.

The synthetic route to prepare all the intermediate and title compounds are shown in Scheme 1.

2. Experimental

2,4-Dihydroxybenzaldehyde, copper(II) acetate monohydrate (Acros), 2-amino-6-methoxybenzothiazole (Aldrich), palladium(II) acetate (Merck), potassium carbonate (System), 1-bromooctane, 1-bromodecane, 1-bromododecane, 1-bromotetradecane, 1-bromohexadecane (Merck) were used without further purification.

2.1. Synthesis of 6-methoxy-2-(2,4-dihydroxybenzylideneamino) benzothiazole

The synthesis of 6-methoxy-2-(2,4-dihydroxybenzylideneamino)benzothiazole is similar to that reported in the literature published by Ha and co-worker in 2010 [9].

*2.2. Synthesis of 6-methoxy-2-(4-alkoxy-2-hydroxybenzylideneamino) benzothiazole, **1a–1e***

0.50 g (1.7 mmol) of 6-methoxy-2-(2,4-dihydroxybenzylideneamino)benzothiazole in acetone was treated with two equivalent of potassium carbonate. To this mixture, 2.2 equivalent of appropriate 1-bromoalkane were added with the temperature maintained at 60 °C and the reaction mixture was heated for overnight under continuous stirring. The resulting mixture was left for evaporation at room temperature. The potassium carbonate was then dissolved in water and separated from the crude precipitate via filtration. The product thus obtained was subsequently purified with *n*-hexane via recrystallisation.

The yield and elemental analysis data for complexes **1a–1e** are summarised as follow:

1a: Yield 46%. Analysis: calculated for $C_{23}H_{27}N_2O_3S$. C 67.12, H 6.61, N 6.81%; found C 67.48, H 6.67, N 6.91%.
1b: Yield 52%. Analysis: calculated for $C_{25}H_{31}N_2O_3S$. C 68.30, H 7.11, N 6.37; found C 68.47, H 7.08, N 6.39%.
1c: Yield 50%. Analysis: calculated for $C_{27}H_{35}N_2O_3S$. C 69.35, H 7.54, N 5.99%; found C 69.68, H 7.71, N 6.01%.
1d: Yield 53%. Analysis: calculated for $C_{29}H_{39}N_2O_3S$. C 70.27, H 7.93, N 5.65%; found C 70.53, H 7.89, N 5.63%.
1e: Yield 50%. Analysis: calculated for $C_{31}H_{43}N_2O_3S$. C 71.09, H 8.27, N 5.35%; found C 71.32, H 8.26, N 5.37%.

2.3. Synthesis of bis[6-methoxy-2-(4-alkoxy-2-hydroxybenzylidene amino)benzothiazole]-copper(II) complexes, **2a–2e**

Ligand **1** (1.0 mmol) was dissolved in a round bottom flask containing ethanol solution (50 ml). To this resulting solution, an ethanolic solution (10 ml) of copper(II) acetate (1.0 mmol) was then added dropwise and was refluxed for 6 h at 70 °C. The brown precipitate formed was collected by filtration and recrystallised from chloroform–ethanol (1:1).

The yield and elemental analysis data for Cu(II) complexes **2a–2e** are summarised as follow:

2a: Yield 75%. Analysis: calculated for $C_{45}H_{54}N_4O_6S_2Cu$. C 61.79, H 6.22, N 6.41%; found C 61.47, H 6.33, N 6.52%.
2b: Yield 79%. Analysis: calculated for $C_{49}H_{62}N_4O_6S_2Cu$. C 63.23, H 6.71, N 6.06%; found C 63.10, H 7.12, N 6.20%.
2c: Yield 70%. Analysis: calculated for $C_{53}H_{70}N_4O_6S_2Cu$. C 64.50, H 7.15, N 5.68%; found C 64.18, H 7.29, N 5.78%.
2d: Yield 80%. Analysis: calculated for $C_{57}H_{78}N_4O_6S_2Cu$. C 65.64, H 7.54, N 5.37%; found C 65.43, H 7.74, N 5.41%
2e: Yield 83%. Analysis: calculated for $C_{61}H_{86}N_4O_6S_2Cu$. C 66.66, H 7.89, N 5.10%; found C 66.50, H 8.08, N 5.18%.

2.4. Synthesis of bis[6-methoxy-2-(4-alkoxy-2-hydroxybenzylidene amino)benzothiazole]-palladium(II) complexes, **3a–3e**

An ethanolic solution (10 ml) of palladium(II) acetate (1.0 mmol) was added dropwise to a hot ethanolic solution (50 ml) of ligand **1** (1.0 mmol) in a round bottom flask. The mixture solution was refluxed for 6 h at 70 °C and then cooled to room temperature. The brown precipitate was collected by filtration and subsequently recrystallised from ethanol.

The yield and elemental analysis data for Pd(II) complexes **3a–3e** are summarised as follow:

3a: Yield 86%. Analysis: calculated for $C_{46}H_{54}N_4O_6S_2Pd$. C 59.44, H 5.85, N 6.03%; found C 59.57, H 5.88, N 6.09%.
3b: Yield 85%. Analysis: calculated for $C_{50}H_{62}N_4O_6S_2Pd$. C 60.93, H 6.34, N 5.68%; found C 61.13, H 6.45, N 5.66%.
3c: Yield 85%. Analysis: calculated for $C_{54}H_{70}N_4O_6S_2Pd$. C 62.26, H 6.77, N 5.38%; found C 62.49, H 6.88, N 5.47%.
3d: Yield 87%. Analysis: calculated for $C_{58}H_{78}N_4O_6S_2Pd$. C 63.45, H 7.16, N 5.10%; found C 63.70, H 7.17, N 5.08%.
3e: Yield 87%. Analysis: calculated for $C_{62}H_{86}N_4O_6S_2Pd$. C 64.53, H 7.51, N 4.85%; found C 64.86, H 7.72, N 4.96%.

2.5. FTIR measurement

The FTIR data were recorded using a Perkin Elmer 2000-FTIR spectrophotometer in the frequency range 4000–400 cm^{-1} with sample prepared in KBr discs.

2.6. NMR measurement

The ^1H and ^{13}C NMR spectra for ligands **1a–1e** and Pd(II) complexes **3a–3e** were obtained using Brucker Avance 300 and 400 MHz ultrashield spectrometers equipped with ultrashield magnets. Standard Bruker pulse programs were used throughout the entire experiment [10]. The ^1H and ^{13}C NMR data for ligands were further substantiated with the aids of 2D ^1H–^1H correlation spectroscopy (COSY), ^1H–^{13}C heteronuclear multiple quantum correlation (HMQC) and ^1H–^{13}C heteronuclear multiple bond correlation (HMBC). Deuterated chloroform ($CDCl_3$) and dimethysulphoxide (DMSO-d_6) were used as solvent and TMS as internal standard.

2.7. Phase transition temperature and enthalpy values

The phase transition temperatures and enthalpy values were measured by using a Seiko DSC6200R calorimeter with the heating and cooling rate of ±5 °C min^{-1}.

2.8. Texture observation

The texture was observed using a Carl Zeiss Axioskop 40 polarising microscope equipped with a Linkam LTS 350 hot stage and TMS94 temperature controller. The samples studied by optical microscope were prepared in thin film sandwiched between glass slide and cover.

2.9. X-ray data collection, structure solution and refinement for ligand **1a**

The X-ray crystal structure analytical data were collected by using a Rigaku Saturn 70 diffractometer, which uses graphite monochromated Mo Kα radiation. The data were collected at a temperature of -159 ± 1 °C to a maximum 2θ value of 55.0°. A total of 720 oscillation images were collected. A sweep of data was done using ω oscillations from -110.0 to 70.0° in 0.5° steps. The exposure rate was 128.0 [s/°]. The detector swing angle was -20.05°. A second sweep was performed using ω oscillations from -110.0° to 70.0° in 0.5° steps. The exposure rate was 128.0 [s/°]. The detector swing angle was -20.05°. The crystal-to-detector distance is 45.32 mm. Readout was performed in the 0.137 mm pixel mode. Out of the 7876 reflections that were collected, 4442 were unique ($R_{int} = 0.0372$); equivalent reflections were merged. Data were collected and processed using CrystalClear (Rigaku). The linear absorption coefficient, μ, for Mo Kα radiation was 1.827 cm^{-1}. An empirical absorption correction was applied which resulted in transmission factors ranging from 0.576 to 0.968. The data were corrected for Lorentz and polarisation.

The structure was solved by direct methods [11] and expanded using Fourier techniques. The non-hydrogen atoms were refined anisotropically. Hydrogen atoms were refined using the riding model. The final cycle of full-matrix least-squares refinement on F^2 was based on the 4442 observed reflections, 374 variable parameters and converged (largest parameter shift was 0.00 times its esd) with unweighted and weighted agreement factors of

$$R_1 = \sum ||F_o| - |F_c|| / \sum |F_o| = 0.0731$$

$$wR_2 = \left[\sum\left(w\left(F_o^2 - F_c^2\right)^2\right)\Big/\sum w\left(F_o^2\right)^2\right]^{1/2} = 0.2184$$

The standard deviation of an observation of unit weight was 1.08. Unit weights were used. The maximum and minimum peaks on the final difference Fourier map corresponded to 0.98 and −0.77 e/Å^3, respectively. Neutral atom scattering factors were taken from Cromer and Waber [12]. Anomalous dispersion effects were included in Fcalc [13]; the values for Δf′ and Δf″ were those of Creagh and McAuley [14]. The values for the mass attenuation coefficients were those of Creagh and Hubbell [15]. All calculations were performed using the Crystal Structure crystallographic software package except for the refinement, which were performed using SHELXL-97 [16].

3. Results and discussion

3.1. IR spectroscopy

The FT-IR spectrum of ligand **1c** shows a broad absorption assignable to the stretching of OH at 3113–3716 cm^{-1} while those of the alkyl groups are observed at 2850–2953 cm^{-1}. A strong absorption band that is observed at 1604 cm^{-1} can be ascribed to the stretching of imine C=N group in the benzothiazole ring. This band is overlapped with the stretching vibration for C=C [9,17]. Besides, the band at 1592 cm^{-1} can also be assigned to the stretching vibration of C=C group in aromatic ring. Another imine C=N group which is obtained from the condensation reaction between 2,4-dihydroxybenzaldehyde and 2-amino-6-methoxybenzothiazole gives rise to the stretching vibration at 1638 cm^{-1} [17,18]. The medium band at 1273 cm^{-1} is attributed to the stretching vibration of C—O phenolic group [19] whereas the band assignable to the stretching vibration of C—O ether is observed as a strong intensity band at 1226 cm^{-1} [20]. The presence of stretching vibration of C—O ether has further confirmed the success of the Williamson etherification reaction with 1-bromododecane [21]. The FT-IR spectra for **1a**, **1b**, **1d** and **1e** show the similar bands as observed in **1c**.

All Cu(II) complexes **2a–2e** and Pd(II) complexes **3a–3e** show similar pattern of FT-IR spectra. Hence, the discussion based on a representative Cu(II) complex **2e** will be reported herein. The spectrum for complex 2**e** (Fig. 1) shows the overlapping of the absorption band for the imine (C=N) group with the absorption band arising from the C=N stretching in the benzothiazole ring results in a sharp and strong absorption band at 1609 cm^{-1}. This observation shows that the stretching frequency of the C=N is shifted to a lower wavenumber in comparison to the free ligand after coordination. One of the reason for this shifting is the coordination of non-bonding electron from N atom to the Cu(II) ion which led to the reduction of the double bond character of C=N [4,17,18,22,1,23]. On the other hand, the absence of the OH band of the free ligands and the shifting of phenolic C—O to a higher frequency at 1313 cm^{-1} in the complexes indicate the deprotonation of OH group and the coordination of O^{-} to the Cu(II) ion [18,19,22,1,23–25]. The other major bands as observed at 2922–2852 cm^{-1} can be assigned to the stretching frequency of C—H bond from alkoxy chain.

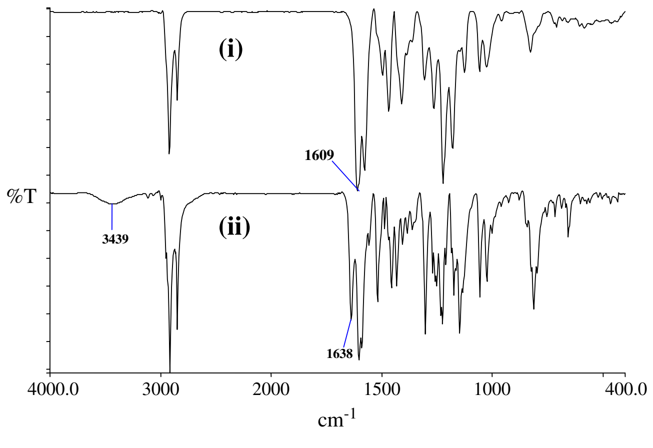

Fig. 1. Representative IR spectrum of (i) Cu(II) complex **2e** and (ii) ligand **1e**.

3.2. NMR spectroscopy

3.2.1. ^{1}H and ^{13}C NMR assignments for ligands *1a–1e*

Based on a representative ligand **1c**, a complete assignment for the title compounds can be described. The ^{1}H NMR spectrum (Table 1) of ligand **1c** is observed in the range of δ = 0.88–12.65 ppm. It can be observed that the signal at δ = 12.65 ppm is attributed to hydroxyl proton, H7. The downfield shift of the hydroxyl proton indicates the presence of intramolecular hydrogen bonding [26] and this observation is in agreement with the crystal structure of 6-methoxy-2-(4-octyloxy-2-hydroxybenzylideneamino)benzothiazole in Section 3.4. The chemical shift for aromatic proton H6 is observed at δ = 7.28–7.29 ppm. As for the azomethine proton H9, it resonates as a singlet at δ = 9.07 ppm. Whereas the proton at δ = 3.89 ppm can be assigned for the proton from methyl group, H8.

The correlation of ^{1}H–^{1}H from COSY experiment of ligand **1c** is employed to assign the aromatic protons. From the COSY spectrum in Fig. 2, the doublet observed at δ = 7.81–7.84 ppm suggests the existence of proton H4 and this proton is correlated with proton H5 which is observed as doublet of doublet at δ = 7.05–7.08 ppm. Another doublet attributed to proton H3 is observed at δ = 7.35–7.37 ppm and is correlated with multipletes observed at δ = 6.50–6.54 ppm for proton H1. Besides, the multipletes that are observed in this range can also be attributed to proton H2 which is due to the overlap of peaks from these two protons. Fig. 1 also shows that the ether group of proton H1′ is observed as triplet at δ = 4.00–4.03 ppm. This proton shows a correlation with the adjacent proton H2′ which is observed as multipletes. A similar correlation is observed for the other homologous members.

All ligands **1a–1e** show a similar pattern in ^{13}C NMR spectra. Hence, a representative ligand **1c** will be discussed. The ^{13}C NMR signals have further been substantiated by DEPT 135, 90 and 45 where the assignment can be governed by the additive rules and substitution effect. Based on the ^{13}C NMR spectroscopy as shown in Table 2 for **1c**, the signal of carbon attached to N atom in the azomethine is observed at δ = 164.77 ppm. The signals at δ = 165.67 and 167.46 ppm can be attributed to C12 and C13, respectively, whereas the resonances for carbons C7 and C11 appear at δ = 165.39 and 157.89 ppm. The signal observed at δ = 146.27 ppm is assigned to carbon C14. The resonances due to the aromatic carbons C1, C2 and C3 are found at δ = 109.16, 101.82 and 135.56 ppm, respectively. Other resonances due to aromatic carbons C4, C5 and C6 are observed at δ = 123.64, 116.05 and 104.76 ppm, respectively. The signals appear at δ = 135.82 and 112.66 ppm can be assigned to respective C10 and C15. For the carbon C8 in the methyl group, it gives rise to a peak at δ = 56.03 ppm. At δ = 14.52 and 32.32 ppm, the signals can be assigned as carbon C (methyl) and C2′, respectively. The δ = 68.85 ppm indicates methyl carbon C1′ of the alkanoyloxy chain.

The HMQC spectra confirm the attachment of different aromatic hydrogens to the respective carbons as discussed in the earlier part on the ^{1}H–^{1}H homonuclear correlation. From Fig. 3, the aromatic carbon atoms for C1, C2, C3, C4, C5 and C6 show a cross peak with proton H1, H2, H3, H4, H5 and H6, respectively. In the same way, the azomethine carbon C9 shows a correlation with proton H9.

Table 1
^{1}H NMR chemical shifts, δ (ppm) of ligands **1a–1e**.

Atom	Chemical shift, δ (ppm)				
	1a	**1b**	**1c**	**1d**	**1e**
H1 and H2	6.52–6.55 (m)	6.51–6.55 (m)	6.50–6.54 (m)	6.50–6.55 (m)	6.52–6.54 (m)
H3	7.34–7.36 (d)	7.35–7.38 (d)	7.35–7.37 (d)	7.36–7.38 (d)	7.35–7.38 (d)
H4	7.81–7.82 (d)	7.81–7.84 (d)	7.81–7.84 (d)	7.81–7.83 (d)	7.81–7.83 (d)
H5	7.06–7.07 (dd)	7.06–7.09 (dd)	7.05–7.08 (dd)	7.06–7.09 (dd)	7.07–7.08 (dd)
H6	7.27–7.28 (s)	7.28–7.29 (s)	7.28–7.29 (s)	7.28–7.29 (s)	7.26–7.29 (s)
H7	12.65 (s)	12.65 (s)	12.65 (s)	12.65 (s)	12.64 (s)
H8	3.91 (s)	3.90 (s)	3.89 (s)	3.90 (s)	3.88 (s)
H9	9.08 (s)	9.07 (s)	9.07 (s)	9.09 (s)	9.06 (s)
H1′	4.02–4.05 (t)	4.00–4.03 (t)	4.00–4.03 (t)	4.02–4.05 (t)	3.99–4.03 (t)
H2′—H*n*′	1.77–1.83 (m)	1.78–1.82 (m)	1.78–1.82 (m)	1.79–1.85 (m)	1.70–1.80 (m)
H (methyl)	0.88–0.91 (t)	0.87–0.90 (t)	0.88–0.89 (t)	0.89–0.93 (t)	0.88–0.90 (t)

TMS as internal standard.
s, Singlet; d, doublet; dd, doublet of doublet; m, multiplets; t, triplet.

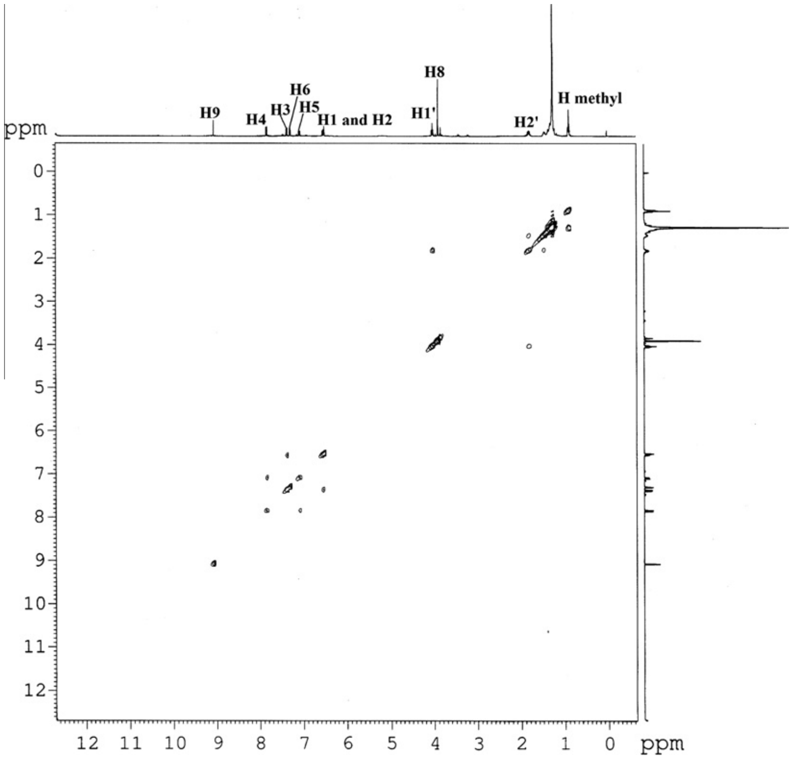

Fig. 2. ^{1}H–^{1}H connectivities in the COSY spectra for ligand **1c**.

Moreover, ^{13}C ^{1}H NMR spectra also indicate the correlation of carbon C8, C1′, C2′ and C12′ with proton H8, H1′, H2′ and H12′.

The HMBC experiment has further confirmed the assignment of quaternary carbons which is established throughout the connectivities between the carbon and its neighbouring proton. Fig. 4 show that the proton H5 is correlated with carbon C10 and C14 with respective ^{2}J and ^{4}J long range connectivities. Similarly, the HMBC spectra also indicate that the H4 has ^{2}J connectivities with quaternary carbon C11 and ^{3}J long range connectivities with quaternary carbon C10. However, the same spectra show that the proton H6 is correlated with carbon C14 and C10 with ^{2}J connectivities. Besides, H6 also shows a cross peak with carbon C5 with ^{3}J long range connectivities. A similar observation can also be observed for azomethine proton H9 which shows a correlation between the quaternary carbon C15 with carbons C3 and C7 by ^{2}J and ^{3}J long range connectivities. The proton H3 shows a cross peak with C1 and C15 with ^{2}J. In addition, the cross peaks of proton H1 and H2 with C3, C7, C12 and C15 further supports the ^{2}J and ^{3}J long range connectivities.

3.2.2. ^{1}H and ^{13}C NMR assignment for Pd(II) complexes *3a–3e*

The resonances in relation to the ^{1}H and ^{13}C NMR of Pd(II) complexes **3a–3e** show a significantly shift to higher or lower field as compared to the uncoordinated ligands **1a–1e**. A representative Pd(II) complex of **3a** will be discussed.

Table 3 shows that the proton H1 is observed as doublet of doublet at δ = 6.19–6.21 ppm while the resonance for proton H2 is obtained as singlet at δ = 5.55 ppm. The chemical shifts for these two protons are shifted to upper field as compared to uncoordinated ligands. In addition, the overlapping of signals for these two protons in the free ligands is not observed in complex **3a**. Table 3 also shows that the singlet at δ = 8.06 ppm can be attributed to the

Table 2
^{13}C NMR chemical shifts, δ (ppm) of compound ligands **1a–1e**.

Atom	Chemical shift, δ (ppm)				
	1a	**1b**	**1c**	**1d**	**1e**
C1	109.15	109.16	109.16	109.15	109.15
C2	101.84	101.80	101.82	101.83	101.82
C3	135.52	135.57	135.56	134.57	135.55
C4	123.67	123.62	123.64	122.63	123.64
C5	116.04	115.03	116.05	116.02	116.02
C6	104.74	104.72	104.76	104.74	104.74
C7	165.38	165.39	165.39	165.40	165.41
C8	56.03	56.02	56.03	56.02	56.04
C9	164.77	164.77	164.77	164.78	164.77
C10	135.83	135.83	135.82	136.81	135.83
C11	157.88	157.87	157.89	157.88	157.88
C12	165.66	165.67	165.67	165.66	166.65
C13	167.45	167.45	167.46	167.45	167.46
C14	146.28	146.28	146.27	146.27	146.27
C15	112.66	112.67	112.66	112.67	112.66
C1′	68.82	68.84	68.85	68.85	68.85
C2′—Cn′	32.30–23.09	32.31–23.06	32.32–23.09	32.30–23.09	32.32–23.10
C (methyl)	14.48	14.51	14.52	14.50	14.49

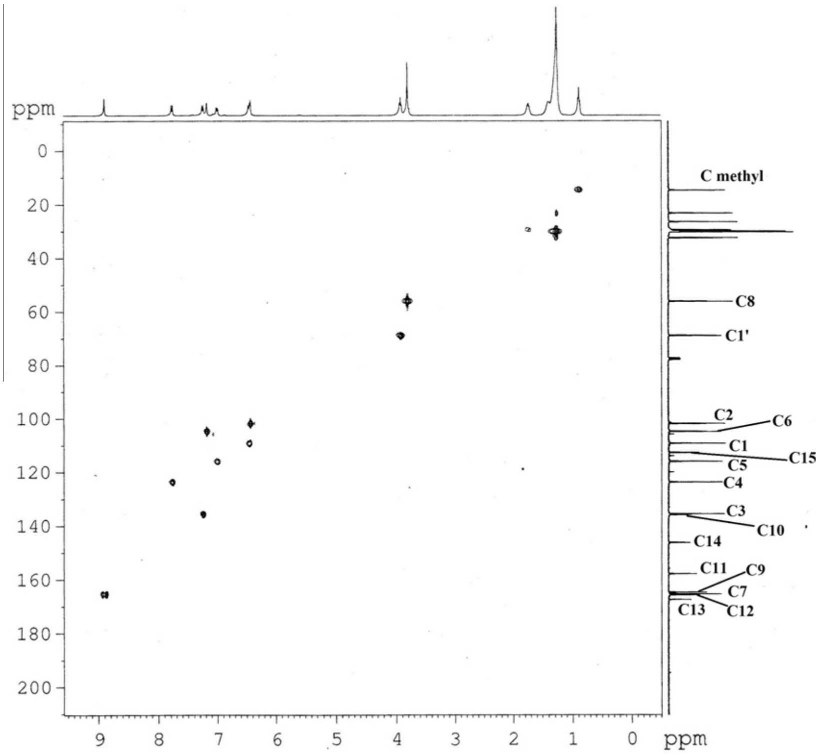

Fig. 3. One bond C—H correlation in the HMQC spectra of ligand **1c**.

proton H9. As compared with the uncoordinated Schiff base **1a** at δ = 9.08 ppm, the chemical shift for this proton is shifted to upper field. Another doublet of doublet signal at δ = 7.10–7.13 ppm indicates the proton H5 while the two doublet signals at δ = 7.31–7.32 ppm and δ = 7.90–7.92 ppm can be assigned to H3 and H4, respectively. The proton H3 and H4 are shifted to upper field whereas the proton H5 is shifted to the lower side as compared to the free ligand **1a**.

The large upfield shifting of the protons (H1, H2, H3 and H9) close to the Pd(II) centre ion are due to the increase of shielding effect that is presumably caused by the π back-bonding from Pd(II) ion [27]. Besides, the absence of phenolic proton H7 and the larger upper shift in chemical shift for H9 further confirm the formation of new Pd—N and Pd—O bonds in Pd(II) complexes [28,29]. These results are in agreement with the molecular structure deduced from FT-IR and CHN data.

The chemical shifts of ^{13}C NMR for Pd(II) complex **3c** are collated in Table 4. The resonance at δ = 167.24 ppm can be ascribed to the carbon C7, in which carbon C7 is the carbon bonded to O and coordinated to Pd(II) ion. The resonance for carbon C1 appears at δ = 109.04 ppm and resonances for C2, C3, C4, C5 and C6 are observed at δ = 102.60, 136.78, 123.84, 115.51 and 104.73 ppm, respectively. These are the resonances due to the aromatic C—H carbons. The resonance observed at δ = 56.23 ppm can be attributed to the carbon C8. The resonance obtained at δ = 167.11 ppm is identified as the carbon C9 whereas the resonance for carbon C1′ from

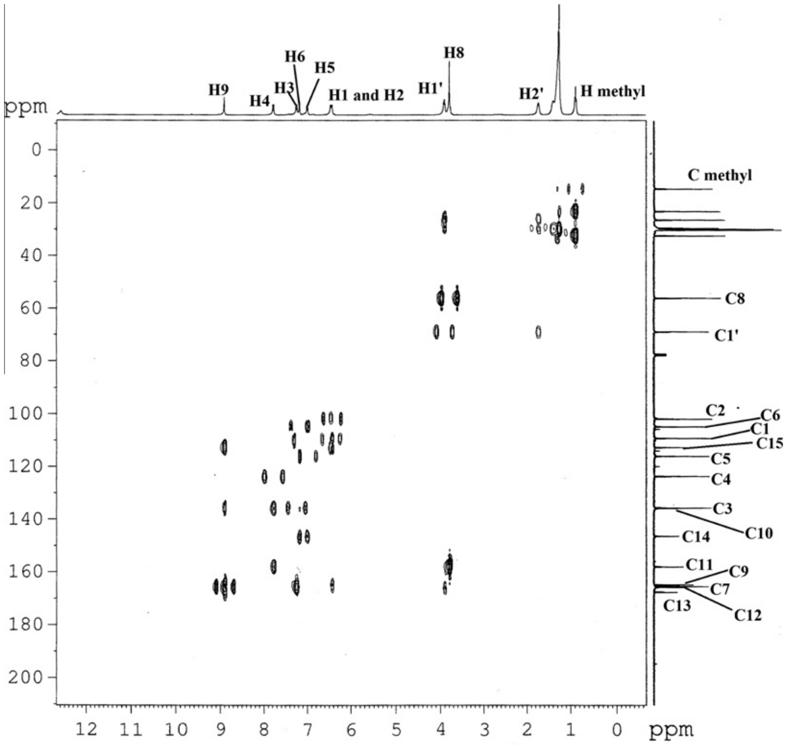

Fig. 4. Long range C—H correlation in the HMBC spectra for ligand **1c**.

Table 3
^{1}H NMR chemical shifts, δ (ppm) of Pd(II) complexes, **3a–3e**.

Atom	Chemical shift, δ (ppm)				
	3a	**3b**	**3c**	**3d**	**3e**
H1	6.19–6.21 (dd)	6.18–6.20 (dd)	6.19–6.21 (dd)	6.18–6.21 (dd)	6.19–6.22 (dd)
H2	5.55 (s)	5.54 (s)	5.55 (s)	5.53 (s)	5.55 (s)
H3	7.31–7.32 (d)	7.31–7.32 (d)	7.30–7.32 (d)	7.31–7.33 (d)	7.30–7.32 (d)
H4	7.90–7.92 (d)	7.90–7.91 (d)	7.91–7.93 (d)	7.90–7.93 (d)	7.90–7.93 (d)
H5	7.10–7.13 (dd)	7.10–7.13 (dd)	7.11–7.14 (dd)	7.10–7.14 (dd)	7.10–7.13 (dd)
H6	7.15 (s)	7.15 (s)	7.14 (s)	7.13 (s)	7.14 (s)
H7	–	–	–	–	–
H8	3.91 (s)	3.91 (s)	3.92 (s)	3.92 (s)	3.91 (s)
H9	8.06 (s)	8.05 (s)	8.06 (s)	8.05 (s)	8.07 (s)
H1′	3.62–3.65 (t)	3.61–3.65 (t)	3.60–3.64 (t)	3.61–3.64 (t)	3.62–3.65 (t)
H2′—H*n*′	1.22–1.69 (m)	1.21–1.68 (m)	1.22–1.69 (m)	1.21–1.67 (m)	1.22–1.69 (m)
H (methyl)	0.90–0.93 (t)	0.91–0.93 (t)	0.90–0.93 (t)	0.91–0.93 (t)	0.91–0.93 (t)

TMS as internal standard.
s, Singlet; d, doublet; dd, doublet of doublet; m, multiplets; t, triplet.

ether group is observed at $\delta = 68.35$ ppm. The resonance at $\delta = 14.18$ ppm can be assigned to the methyl carbon C12′. On the other hand, the resonances for quaternary aromatic carbons C10, C11, C12, C13, C14 and C15 are observed at $\delta = 137.16$ ppm, 158.14 ppm, 167.57 ppm, 169.38 ppm, 146.67 ppm and 115.28 ppm, respectively. The other homologous members of Pd(II) complexes show the similar pattern of ^{13}C NMR as described for complex **3c**.

3.3. *Mesomorphic behaviour*

The observation from polarising microscope and DSC traces revealed that all the uncoordinated ligands are enantiotropic whereas all the corresponding Cu(II) and Pd(II) complexes are non mesogenic. The transitions temperatures and associated enthalpies (kJ mol^{-1}) of the ligands (**1a–1e**) with their corresponding Cu(II) and Pd(II) complexes are shown in respective Tables 5–7.

All the ligands are nematogenic. The thermal behaviours of the ligands **1a–1e** are similar as we can infer from the DSC curve. Therefore, the ligand **1b** will be discussed as a representative example. The heating cycle of ligand **1b** exhibits two endothermic peaks at 81.5 °C and 127.7 °C, respectively. The first transition corresponds to the transition of crystal to nematic phase (Cr—N) with the associated enthalpies 29.96 kJ mol^{-1} followed by the transition to isotropic phase which gives the second endothermic peak. The cooling cycle of ligand **1b** exhibits two exothermic transitions at 125.9 °C and 58.0 °C corresponding to the transitions of I—N and N—Cr.

Texture observation under polarising microscope reveals that the ligands **1a–1e** exhibit schlieren textures of N phase with

Table 4
^{13}C NMR chemical shift (ppm) of Pd(II) complexes **3a–3e**.

Atom	Chemical shift, δ (ppm)				
	3a	**3b**	**3c**	**3d**	**3e**
C1	109.02	109.00	109.04	109.02	108.95
C2	102.58	102.56	102.60	102.60	102.58
C3	136.86	136.88	136.78	136.79	136.79
C4	123.83	123.85	123.84	123.83	123.79
C5	115.41	115.44	115.51	115.52	115.42
C6	104.69	104.70	104.73	103.70	104.74
C7	167.24	167.26	167.32	167.25	167.24
C8	56.18	56.20	56.23	56.28	56.13
C9	162.14	167.10	167.11	167.17	167.15
C10	137.10	137.13	137.16	137.14	137.13
C11	158.14	158.13	158.14	158.13	158.14
C12	167.55	167.56	167.57	167.53	167.55
C13	169.33	169.35	169.38	169.33	169.35
C14	146.68	146.68	146.67	146.68	146.67
C15	115.29	115.30	115.28	115.30	115.29
C1′	68.37	68.34	68.35	68.35	69.15
C2′—Cn′	22.88–32.07	22.88–32.06	22.86–32.03	22.88–32.09	22.87–32.05
C(methyl)	14.19	14.20	14.18	14.20	14.19

Table 5
Phase transition temperatures (°C) and associated enthalpies (kJ mol^{-1}) of ligands **1a** (n = 8) to **1e** (n = 16).

Ligands		Cr$_1$		Cr$_2$		N	I	
1a	Heating	•	88.5 (42.67)			•	145.0[a]	•
	Cooling	•	73.7 (−36.9)			•	142.9[a]	•
1b	Heating	•	81.5 (29.96)			•	127.3[a]	•
	Cooling	•	58.0 (−19.3)			•	125.9[a]	•
1c	Heating	•	81.5 (14.92)	•	84.7 (30.5)	•	122.7[a]	•
	Cooling	•	68.3 (−31.6)	•	96.1[a]	•	121.8[a]	•
1d	Heating	•	72.4 (12.43)	•	87.2 (22.15)	•	120.9[a]	•
	Cooling	•	69.8[a]	•	72.4[a] (−34.1)	•	118.7[a]	•
1e	Heating	•	93.2 (34.83)			•	104.0[a]	•
	Cooling	•	79.8 (−34.0)			•	103.2[a]	•

Cr, crystal; N, nematic; I, isotropic.
[a] Denotes transition temperature derived from unresolved peaks.

Table 6
Phase transition temperatures (°C) and associated enthalpies (kJ mol^{-1}) of complexes **2a–2e**.

Complexes		Cr$_1$		I
2a	Heating	•	189.2 (49.3)	•
2b	Heating	•	181.7 (33,5)	•
2c	Heating	•	172.5 (18.9)	•
2d	Heating	•	163.4 (35.9)	•
2e	Heating	•	154.4 (49.5)	•

Cr, crystal; I, isotropic.

Table 7
Phase transition temperature (°C) and associated enthalpies (kJ mol^{-1}) of complexes **3a** (n = 8) to **3e** (n = 16).

Complexes		Cr	I	
3a	Heating	•	220.36 (26.6)	•
3b	Heating	•	215.62 (25.1)	•
3c	Heating	•	199.51 (31.7)	•
3d	Heating	•	189.35 (25.8)	•
3e	Heating	•	180.5[a]	•

Cr, crystal; I, isotropic.
[a] Denotes transition temperature derived from unresolved peaks.

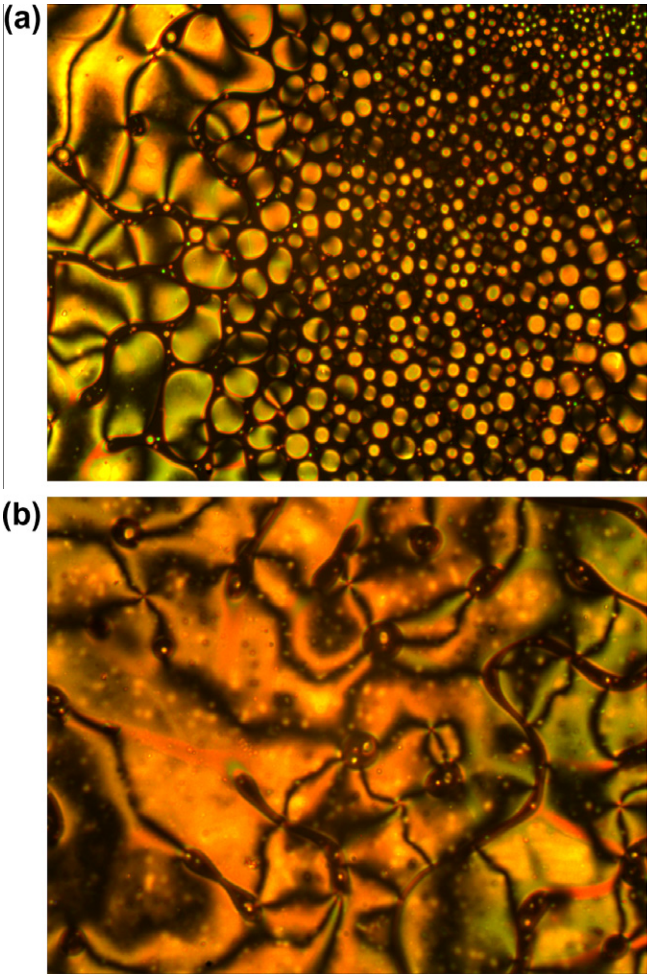

Fig. 5. Photomicrographs of ligand **1c** upon cooling. (a) The small droplets characteristics of the nematic phase; and (b) the schlieren texture of nematic phase with two-brush and four-brush defects. Cr, crystal; N, nematic; I, isotropic; L, ligands; CuL2; Cu(II) complexes; PdL2; Pd(II) complexes.

two-brush and four-brush defects [9]. Upon cooling from isotropic liquid, the nematic droplets appear and coalesces (Fig. 5a) to form the classical schlieren texture with two-brush and four-brush defects (Fig. 5b) [9]. This nematic phase is reproducible upon continuous heating and cooling.

Fig. 6 illustrates the correlation of phase transition temperatures and the carbon number of the flexible chain in uncoordinated ligands. The clearing points of the ligands are considerably reduced upon increasing the number of carbon in the alkoxy chain from $n = 8$ to $n = 16$. This observation is resulted from the dilution of core system induced by the increasing of the flexibility of the terminal alkoxy chain [30,31]. On the other hand, this figure clearly shows that the nematic phase range begins to drop upon lengthening of the alkoxy chain from $n = 8$ to $n = 16$ [31].

However, all the Cu(II) complexes **2a–2e** and Pd(II) complexes **3a–3e** do not exhibit liquid crystalline properties even though their ligands are nematogenic. Optical observation shows that these complexes are clearly melted and transformed into isotropic phase. Besides, continuous heating after the melting point causes the immediate decomposition which appears to be extinct black under the polarising light. On the other hand, the first heating cycle of DSC curve for this two series of complexes exhibit only one endothermic transition whereas during the cooling cycle there is no exothermic transition observed due to the thermal decomposition occurs during the first heating cycle.

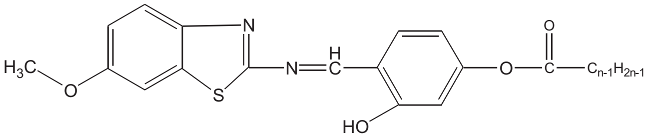

nMHBABTH

where n= 8, 10, 12, 14, 16

The greater polarity of the coordination bond and the differences in the molecular geometry between ligands and metal complexes could probably be the reason for the suppression of N phase in the Cu(II) and Pd(II) complexes [23]. Besides, another reason is the structural orientation and hydrophobicity of the Cu(II) and Pd(II) complexes which do not favour the mesogenic character [4]. On the other hand, Fig. 6 shows that the clearing temperatures of Cu(II) and Pd(II) complexes are significantly higher in comparison with the free ligands **5a–5e**. This could be resulted from the increase in their molecular weights and the number of interacting sites upon complexes formation [32]. However, Pd(II) complexes **3a–3e** have relatively higher clearing temperatures as compared to those values in Cu(II) complexes **2a–2e** (Fig. 6). This is not surprising as the molecular weight of Pd(II) ion is higher than Cu(II) analogue and is also due to the possibility of the presence of weak Pd—Pd intermolecular interaction [32].

3.3.1. Chemical structure–mesomorphic property relationship

The homologous series of benzothiazole-cored Schiff bases **1a–1e** are compared to the structurally related compounds reported by Ha and co-worker in 2010 with general structure as shown below [9]. Only compounds **8MHBABTH** to **16MHBABTH** are chosen to compare with **1a–1e** to ensure that the comparison is relevant. The comparison will be discussed in term of transition temperature, type of mesophase, mesophase range and molecular structures.

Both series have almost similar molecular structure but with a different functional group at the terminal chain. Compounds **8MHBABTH** to **16MHBABTH** contain an ester linkage at the terminal flexible chain whereas present ligands **1a–1e** contain an ether linkage. It is found that although both series exhibit N phase but compounds **8MHBABTH** to **16MHBABTH** show a marble texture of N phase which are different from schlieren textures observed in **1a–1e**. Comparing the transition temperatures and mesophase range of compounds **8MHBABTH** to **16MHBABTH** and **1a–1e** reveals that compounds **8MHBABTH** to **16MHBABTH** possess higher clearing temperatures. However, **1a–1e** have relatively larger N phase range as compared to compounds **8MHBABTH** to **16MHBABTH.** All these observation are due to the greater polarity of ester linkages compared to ether linkage.

Compound	Transition temperatures (°C)	Mesophase range (°C)
8 MHBABTH	Cr 133.2 N 145.8 I	12.6
10 MHBABTH	Cr 127.5 N 139.5 I	12.0
12 MHBABTH	Cr 124.9 N 136.8 I	11.9
14 MHBABTH	Cr 123.6 N 133.6 I	10.0
16 MHBABTH	Cr 123.2 N 129.7 I	6.5

3.4. Crystal structure of 6-methoxy-2-(4-octyloxy-2-hydroxybenzylideneamino)-benzothiazole, *1a*

The molecular structure with the atom-numbering scheme of 6-methoxy-2-(4-octyloxy-2-hydroxybenzylideneamino)benzothiazole, **1a** is shown in Fig. 7. Crystal data and refinement of ligand **1a** are collated in Table 8.

The molecule of 6-methoxy-2-(4-octyloxy-2-hydroxybenzylideneamino)-benzothiazole, **1a** crystallines into triclinic lattice with the space group of P-1. Fig. 7 shows that the discrete molecule of ligand **5a** consists of a benzothiazole moieties linked by an imine linkage to the *ortho*-hydroxyl phenyl ring bearing an alkoxy chain of OC_8H_{17}. The bond lengths for exocyclic imine N2—C9 and imine group N1—C8 in the benzothiazole ring are 1.298 Å and 1.303 Å, respectively. There is no remarkable difference between these two C=N bond distances which resemble the value reported for 2-(2,4-dimethylpyrolly)benzothiazole by Rajnikat and co-worker in which the C=N bond length was 1.284 Å (C=N) [33].

Fig. 7 also shows that the two bulky groups situated at the opposite side of the imine C=N and this led to formation of **E** isomer. The E conformation is preferred because it helps to reduce the crowdiness thus forming a more stable (**E**)-6-methoxy-2-(4-octyloxy-2-hydroxybenzylideneamino)benzothiazole. The bond lengths of two C—S bonds in the five member thiazole ring are 1.734 Å (S1—C3) and 1.745 Å (S1—C8), respectively. On the other hand, the C4—N1—C8 angle in the benzothiazole ring is 109.3 °C. These values are similar to those values reported for 2-(2,4-dimethylpyrolly)benzothiazole [33].

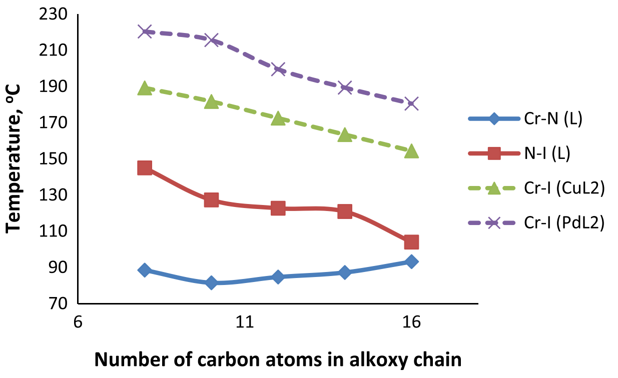

Fig. 6. A plot of phase transition temperature upon heating versus the number of carbon atoms in alkoxy chain for the ligands **1a–1e** (solid line) and their corresponding metal complexes (dotted line). Cr, crystal; N, nematic; I, isotropic; L, ligands; CuL2; Cu(II) complexes; PdL2; Pd(II) complexes.

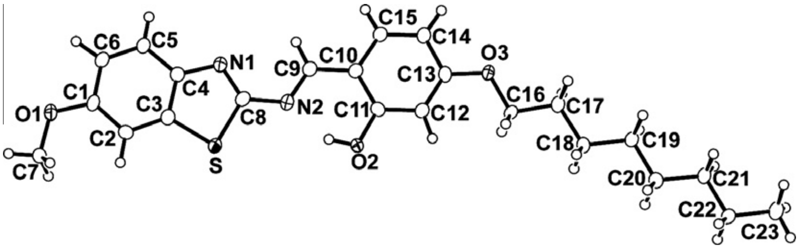

Fig. 7. The molecular structure with the atom-numbering scheme of 6-methoxyl-2-(4-octyloxy-2-hydroxybenzylideneamino)benzothiazole, **1a**.

Table 8
Crystal data and refinement of ligand **1a**.

Crystal data	Values
Empirical formula	$C_{23}H_{28}N_2O_3S$
Formula weight	412.55
Crystal colour, habit	Yellow, prism
Crystal dimensions	0.270 × 0.220 × 0.180 mm
Crystal system	Triclinic
Lattice type	Primitive
Lattice parameters	$a = 5.82880(10)$ Å
	$b = 13.000(3)$ Å
	$c = 15.085(6)$ Å
	$a = 73.97(3)°$
	$b = 79.67(4)°$
	$g = 72.12(4)°$
	$V = 1039.9(5)$ Å^3
Space group	P-1 (#2)
Z value	2
D_{calc}	1.317 g/cm^3
$F000$	440
m(Mo Kα)	1.827 cm^{-1}
Refinement	Full-matrix least-squares on F^2
Function minimised	$\sum w(F_o^2 - F_c^2)^2$
Least squares weights	$w = 1/[\sigma^2(F_o^2) + (0.1117 \cdot P)^2 + 0.0000 \cdot P]$ where $P = (\text{Max}(F_o^2, 0) + 2F_c^2)/3$
$2q_{max}$ cutoff	55.0°
Anomalous dispersion	All non-hydrogen atoms
No. observations (All reflections)	4442
No. Variables	374
Reflection/parameter ratio	11.88
Residuals: $R1$ ($I > 2.00\sigma(I)$)	0.0731
Residuals: R (all reflections)	0.1
Residuals: w$R2$ (all reflections)	0.2184
Goodness of fit indicator	1.076
Max shift/error in final cycle	0.001
Maximum peak in final diff. map	0.98 e/Å^3
Minimum peak in final diff. map	−0.77 e/Å^3

In addition, the existence of intramolecular hydrogen bond O2—H2···N2 in which O2 acts as donor and N2 acts as acceptor is further confirmed by the crystal structure of 6-methoxyl-2-(4-octyloxy-2-hydroxybenzylidene-amino)benzothiazole, **1a**.

Acknowledgements

The main author (G.-Y. Yeap) would like to thank Universiti Sains Malaysia for the RU Grant No. 1001/PKIMIA/811159 and Incentive Grant No. 1001/PKIMIA/822208.

Appendix A. Supplementary material

Table 1 shows the acquisition parameters used in the NMR measurements. The amount of chemicals and solvents used for synthesis are collated in Tables 2–4. The frequencies, ν (cm^{-1}) and relative intensities of the diagnostic bands in the FT-IR spectra for ligands **1a–1e** and their corresponding Cu(II) and Pd(II) complexes are listed in Tables 5–7. Tables 8 and 9 show the ^{1}H–^{1}H COSY, ^{1}H–^{13}C HMQC and HMBC correlation for ligand **1c**. The intensity measurement of **1a** are listed in Table 10. Tables 11, 12 and 13 show the atomic coordinates, B_{iso}/B_{eq}, B_{iso} of ligand **1a** which involved hydrogen atoms and anisotropic displacement parameters. Whilst the selected bond lengths and bond angles are given in Tables 14 and 16, bond lengths and bond angles involving hydrogen are listed in Tables 15 and 17. Supplementary data associated with this article can be found, in the online version, at doi:10.1016/j.molstruc.2011.12.048.

References

[1] Z. Rezvani, B. Divband, A.R. Abbasi, K. Nejati, Polyhedron 25 (2006) 1915–1920.
[2] C.K. Lee, M.C. Ling, J.B. Ivan Lim, J. Chem. Soc., Dalton Trans. (2003) 4731–4737.
[3] E. Meyer, C. Zucco, H.J. Gallardo, J. Mater. 8 (1998) 1351–1354.
[4] D.B. Patel, P.K. Bhattacharya, Mol. Cryst. Liq. Cryst. 432 (2005) 47–57.
[5] S.T. Ha, T.M. Koh, S.L. Lee, G.Y. Yeap, H.C. Lin, S.T. Ong, Liq. Cryst. 37 (2010) 547–554.
[6] J. Belmar, M. Parra, C. Zuniga, C. Perez, C. Munoz, Liq. Cryst. 26 (1999) 386–396.
[7] S.T. Ha, T.M. Koh, H.C. Lin, G.Y. Yeap, Y.F. Win, S.T. Ong, Y. Sivasothy, L.K. Ong, Liq. Cryst. 36 (2009) 917–925.
[8] C. Sekine, N. Konya, M. Minai, K. Fujisawa, Liq. Cryst. 28 (2001) 1361–1367.

[9] S.T. Ha, T.M. Koh, G.Y. Yeap, H.C. Lin, S.L. Lee, Y.F. Win, S.T. Ong, Mol. Cryst. Liq. Cryst. 528 (2010) 10–22.

[10] Bruker program 1D WIN-NMR (release 6.0) and 2D WIN-NMR (release 6.1).

[11] SIR2004: M.C. Burla, R. Caliandro, M. Camalli, B. Carrozzini, G.L. Cascarano, L. De Caro, C. Giacovazzo, G. Polidori, R. Spagna, 2005.

[12] D.T. Cromer, J.T. Waber, International Tables for X-ray Crystallography, vol. IV, The Kynoch Press, Birmingham, England, 1974, Table 2.2A.

[13] J.A. Ibers, W.C. Hamilton, Acta Cryst. 17 (1964) 781.

[14] D.C. Creagh, W.J. McAuley, in: A.J.C. Wilson (Ed.), International Tables for Crystallography, vol. C, Kluwer Academic Publishers, Boston, 1992, Table 4.2.6.8, pp. 219–222.

[15] D.C. Creagh, J.H. Hubbell, in: A.J.C. Wilson, (Ed.), International Tables for Crystallography, vol. C, Kluwer Academic Publishers, Boston, 1992, Table 4.2.4.3, pp. 200–206.

[16] G.M. Sheldrick, Acta Cryst. A 64 (2008) 112–122.

[17] M. Hassan, Z.H. Chohan, C.T. Supuran, Syn. React. Inorg. Met-org. Chem. 32 (2002) 1445–1461.

[18] D. Pucci, I. Aiello, A. Bellusci, G. Callipari, A. Crispini, M. Ghedini, Mol.Cryst. Liq. Cryst. 500 (2009) 144–154.

[19] I.M. Mustafa, M.A. Hapipah, M.A. Abdulla, T.R. Ward, Polyhedron 28 (2009) 3993–3998.

[20] E. Pretsch, P. Buhlmann, Structure Determination of Organic Compound, Spring-Verlag, Berlin, Heidelberg, New York, 2000.

[21] P. Raveendran, B.K. Sadashiva, B.K. Murty, K.V.G.K. Murty, T.K.K. Srinivasan, Mol. Cryst. Liq. Cryst. 363 (2000) 19–34.

[22] Z. Rezvani, L.R. Ahar, K. Nejati, S.M. Seyedahnadian, Acta Chim. Slov. 51 (2004) 675–686.

[23] A. Suste, V. Sunjic, Liq. Cryst. 20 (1996) 219–224.

[24] V.S. Nandiraju, D. Singha, M. Das, M.K. Paul, Mol. Cryst. Liq. Cryst. 373 (2002) 105–117.

[25] B.S. Creaven, B. Duff, D.A. Egan, K. Kavanagh, G. Rosair, V.R. Thangella, M. Walsh, Inorg. Chim. Acta 363 (2010) 4048–4085.

[26] B.I. Ostrovskii, A.S. Rabinovich, E.L. Sonic, B.A. Sorkin, S.A. Strukov, Taraskin, Ferroelectrics 24 (1980) 309.

[27] O.A. Blackburn, B.J. Coe, J. Fielden, M. Helliwell, J.W. McDouall, M.G. Hutchings, Inorg. Chem. 49 (2010) 9236–9250.

[28] K. Dey, S. Sarkar, S. Mukhopadhyay, A.K. Malik, S. Biswas, B.B. Bhaumik, J. Coord. Chem. 11 (2006) 1233–1253.

[29] M. Marcos, J.L. Serrano, T. Sierra, J. Gimenez, J. Chem. Mater. 5 (1993) 1332–1337.

[30] P. Berdague, J.P. Bayle, M.S. Ho, B.M. Fung, Liq. Cryst. 14 (1993) 667–674.

[31] S.T. Ha, T.M. Koh, G.Y. Yeap, H.C. Lin, J.K. Beh, F.Y. Win, P.L. Boey, Chin. Chem. Lett. 20 (2009) 1081–1084.

[32] H.W. Chae, O.N. Kadhin, M.G.J. Choi, Liq. Cryst. 36 (2009) 53–60.

[33] Rajnikant, S. Kohli, M.B. Deshmukh, J. Chem. Crystallogr. 40 (2010) 765–768.